Automatic Region Template Generation for Shape Particle Filtering based Image Segmentation*

Lukas Fischer[1,2], Rene Donner[1,3], Franz Kainberger[1], Georg Langs[4,1]

[1] Medical University of Vienna, Department of Radiology,
Computational Image Analysis and Radiology Lab
{lukas.a.fischer, rene.donner, franz.kainberger,
georg.langs}@meduniwien.ac.at
[2] Vienna University of Technology, Institute of Computer Aided Automation,
Pattern Recognition and Image Processing Group
[3] Graz University of Technology, Institute for Computer Graphics and Vision
[4] Massachusetts Institute of Technology,
Computer Science and Artificial Intelligence Lab

Abstract. Segmentation approaches based on sequential Monte Carlo Methods deliver promising results for the localization and delineation of anatomical structures in medical images. Also known as Shape Particle Filters, they are used for the segmentation of human vertebræ, lungs and hearts, and are especially well suited to cope with the high levels of noise encountered in MR data and overlapping structures with ambiguous appearance in radiographs.
They require a region template of the appearance features which allow to estimate the confidence in the hypotheses generated during the search. Currently these templates are created manually, which introduces a bias, and leads to particularly sub-optimal results in complex anatomy.
In this work we propose a Differential Evolution based Shape Particle Filter segmentation scheme where the optimal distribution and number of template regions is derived automatically from a set of training images. The method adapts to complex data and finds consistent features in the training examples. Experiments on two medical data sets (radiographs of metacarpal bones and MRI slices of hearts) show that this yields considerably higher accuracy with fewer outliers.

1 Introduction

Motivation Statistical methods such as sequential Monte Carlo Methods were proposed for detection, segmentation [1, 2, 3, 4, 5] and tracking [6, 7, 8] of objects. A similar approach, called Shape Particle Filters was introduced in [2, 3] for the segmentation of vertebræ, lungs and hearts. In Fig. 1 an illustration of a Shape Particle Filter approach is depicted: Based on a global shape model

* This work has been supported by the Austrian National Bank Anniversary Fond projects COBAQUO and BIOBONE.

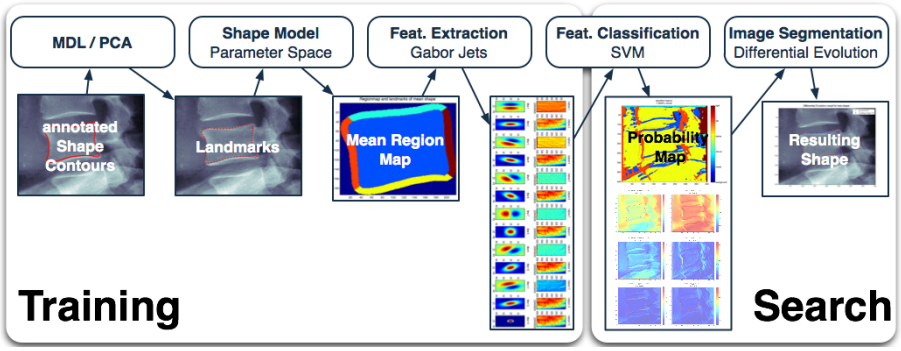

Fig. 1. Flowchart of a Shape Particle Filter. Landmarks are obtained from manually annotated contours, forming the basis for the generated Shape Model. A region map based on the shape models mean shape is generated that in turn is used to determine image region features. Test images are then classified yielding probability maps that are used in the final image segmentation step.

a *class template* or *labeling map* for the following feature extraction is defined according to the respective medical object of interest (e.g. interior of the contour and one or more regions within a certain border on the outside). The number and location of these regions however is currently defined manually. Using these regions and their corresponding distributions in the feature space particle filtering approaches are used to estimate the most probable point in the shape parameter space (corresponding to a segmentation of the image) for a given test image. This is achieved by sampling from the image features according to shape hypothesis and computing corresponding confidence values / posterior probabilities. Estimating this posterior probabilities over the parameter space allows to find values of maximum confidence, i.e. to optimize the fit of the model to the object in the test image.

Particle Filters Particle filtering was introduced with the intention to implement recursive Bayesian filters [9]. It is also known as Sampling Importance Resampling (SIR), Bayesian bootstrap filter or *sequential Monte Carlo Methods*. In contrast to other filters that use Monte Carlo Methods to get estimates of the mean and covariance of the posterior, particle filters approximate the complete posterior. They aim to approximate posterior densities using swarms of points (so called *particles*) in a sample space. A weight is assigned to each particle and using a discrete distribution of the particles the posterior distribution can be approximated. This results in particle probabilities which are proportional to the particle weights. Several algorithms exist differing mainly in the way how the particle swarms evolve and adapt to input data [10].

Contribution In this paper we propose an approach to automatically select the subregions of the object required to compute the expected feature distributions

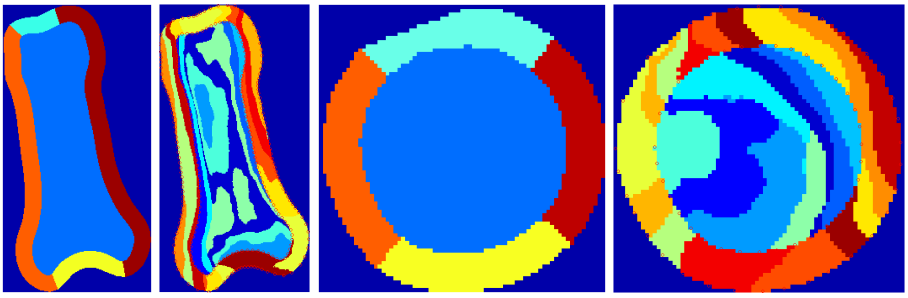

(a) (b) (c) (d)

Fig. 2. Manually predefined region maps (a,c) with five regions and examples of automatically generated region maps (b,d) with 17 (8 inner and 9 outer) regions for the metacarpal bones and the hearts.

and the confidences for each shape hypothesis. The automatic region map is based on the shape of the objects to be classified. Two areas are defined, the interior of the shape and to constrain the representation to a neighborhood of the object a corridor on the outside of the shape. The subregions are estimated for each of the two areas by clustering in feature space.

The optimal number and location of inner and outer regions (clusters) is found by leave one out cross validation. A comparison of manually predefined region maps and examples of automatically generated region maps for each of the processed data sets is shown in Fig. 2. This has several advantages over the manual choice of template regions: the main feature is a partitioning adapted to complex but consistent anatomical structures, which hold information relevant to the segmentation process, but cannot be determined optimally by manual segmentation. It removes bias and finally it opens the possibility of autonomous learning approaches, that do not require manual supervision on a training population.

We evaluate our method on radiographs of human metacarpal bones and MRI slices of human hearts. The results show the drastically improved search results compared to a manual region definition, with both higher accuracy and a smaller number of outliers.

Paper Structure Sec. 2 gives a description of the fundamental methods of the proposed approach, namely the concept of Shape Models 2.1, Differential Evolution 2.2 and the resulting Shape Particle Filter 2.3. Sec. 3 details the automatic region estimation and the experiments and results are presented in Sec. 4 followed by the conclusion and an outlook in Sec. 5.

2 Methods

Shape Particle Filters rely on a model of the objects' shapes and a means of estimating the posterior distribution of parameter estimates given an input im-

age. These are estimated by means of an Markov Chain Monte Carlo (MCMC) method, where Differential Evolution MCMC is used in this work.

2.1 Shape Models

Objects in images can be represented using statistical models of the objects' shape. A Point Distribution Model (PDM) [11] constructs a shape model by computing the significant eigenmodes of a shape population, e. g. assuming a multivariate Gaussian distribution of the shape parameters.

These shapes consist of a set of n points or landmarks. The points can have any dimension, but throughout this paper they are considered to be 2-dimensional. Before modeling the non-rigid shape variation we normalize for similarity transformations, i. e. translation, rotation and scaling (the *pose*). Thus the parameters to define a unique shape in an image are shape and pose parameters.

Using this shape information the goal is to build models which provide the abilities to represent shapes and to generalize to new shapes within the distribution of the shapes in a predefined training set.

The first step to create a training set for shape model generation is to define landmarks for several objects. To obtain landmarks for a shape usually a human expert annotates several images containing the corresponding object. Landmarks are derived from this manually annotated image contours by applying Minimum Description Length (MDL) [12]. Then a vector $\mathbf{v}_i$ for all $i \in 1, ..., N_S$ annotated shapes for d-dimensional landmarks is defined as

$$\mathbf{v}_i = (d_{1_1}, ..., d_{1_d}, d_{2_1}, ..., d_{2_d}, ..., d_{n_1}, ...d_{n_d}) \tag{1}$$

The training set is then aligned using Procrustes Analysis, which minimizes $\sum |\mathbf{v}_i - \bar{\mathbf{v}}|^2$, where $\mathbf{v}_i$ is the i^{th} point position vector and $\bar{\mathbf{v}}$ is the mean of all vectors.

To be able to generate new shapes out of the training set a parameterized model $\mathbf{v} = M(\mathbf{b})$ of the distribution of the N_S point position vectors $\mathbf{v}_i$ is defined. $\mathbf{b}$ is a vector containing the model parameters (Eq. 3). With the help of this model it is possible to generate new shapes $\mathbf{v}$ and to estimate the distribution $p(\mathbf{v})$ of these new vectors. The model is finally built by applying Principle Component Analysis (PCA) to the data, yielding eigenvectors $\mathbf{e}_1, \ldots, \mathbf{e}_e$ with $e = min(nd, N_S)$. Using $e^* < e$ eigenvectors (thereby neglecting the modes with small variance, which are considered to model noise only) any shape $\mathbf{v}$ within the subspace spanned by the training set can be represented by:

$$\mathbf{v} \approx \bar{\mathbf{v}} + \mathbf{F}\mathbf{b} \tag{2}$$

where $\mathbf{F} = (\mathbf{e}_1, ..., \mathbf{e}_{e^*})$ is the basis of the eigenspace and $\mathbf{b}$ is a vector of length e^* which defines the parameters for the deformable model [13]:

$$\mathbf{b} = \mathbf{F}^T(\mathbf{v} - \bar{\mathbf{v}}) \tag{3}$$

The resulting model $\mathbf{F}$ represents the shape variation of the modeled objects utilizing a single parameter vector $\mathbf{b}$. Each element of $\mathbf{b}$ controls one mode of shape variation, with the first modes being responsible for the highest variation, in descending order.

To ensure that the generated shapes are similar to those in the training set the parameter vectors are always limited to the range $\pm 3\sqrt{\lambda_i}$, where λ_i is the eigenvalue and also the variance of the i^{th} parameter b_i in the training set.

In addition to these modes the transformations translation, scaling and rotation need to be taken into account. Therefore a new linear parameter vector $\mathbf{t} = (s_x, s_y, t_x, t_y)^T$ is introduced, controlling rotation θ, scaling s and translation (t_x, t_y), with $s_x = s\cos\theta - 1$ and $s_y = s\sin\theta$.

Combining the parameter vector of the PCA $\mathbf{b}$ and the parameter vector for translation, rotation and scaling $\mathbf{t}$ results in the combined parameter vector

$$\mathbf{c} = (\mathbf{b}^T, \mathbf{t}^T). \tag{4}$$

2.2 Differential Evolution

We approach particle filtering using the DE-MCMC formulation introduced by [14], that uses Differential Evolution (DE) [15] for the sampling step in sequential Monte Carlo Methods. DE is a genetic algorithm and aims to optimize functions based on populations in parameter space, which in our case is the subspace (restricted to plausible models) of the model parameters $\mathbf{c}$.

DE is a parallel direct search method that uses N_x d-dimensional parameter vectors $\mathbf{x}_i$ $(i = 1, ..., N_x)$ (i.e. N_x d-dimensional Markov chains [14]) as members of a population $\mathbf{X}_g$ for each generation g.

Starting with parameter vectors randomly drawn from the training distribution at generation $g = 1$, during each generation $(g + 1)$, N_x new parameter vectors / shape hypotheses $\mathbf{x}^h$ are then generated by adding the weighted difference vector between two population members to a third member

$$\mathbf{x}^h = \mathbf{x}_1 + \gamma(\mathbf{x}_2 - \mathbf{x}_3), \tag{5}$$

where $\mathbf{x}_1, \mathbf{x}_2, \mathbf{x}_3$ are randomly selected without replacement from the population $\mathbf{X}_g$ and γ is a constant factor weighting the differential variation $\mathbf{x}_2 - \mathbf{x}_3$ ($\gamma = 0.85$ in our experiments). If the confidence $\pi(\mathbf{x}^h)$ in hypothesis $\mathbf{x}^h$ is higher than $\pi(\mathbf{x}_1)$, $\mathbf{x}^h$ replaces $\mathbf{x}_1$ in generation $\mathbf{X}_{g+1}$, otherwise $\mathbf{x}_1 \in \mathbf{X}_{g+1}$. After I iterations ensuring convergence (200 in our experiments) the hypothesis / population member $\mathbf{x}^*$ with the highest confidence is considered to represent the best solution.

To guarantee a detailed balance of proposal and acceptance with respect to the fitness function $\pi(.)$ Eq. 5 is modified to

$$\mathbf{x}^h = \mathbf{x}_1 + \gamma(\mathbf{x}_2 - \mathbf{x}_3) + \mathbf{k} \tag{6}$$

where $\mathbf{k}$ is drawn from the normal distribution $\mathbf{k} \sim N(0, \mathbf{a})$ with variance $\mathbf{a}$ small compared to the variance of population $\mathbf{X}_g$ [14].

2.3 Shape Particle Filter

Shape Particle Filters as proposed in [2, 3] contain the following steps. First the mean shape is derived from hand annotated training images. Then a region map is manually defined on this mean shape, representing regions which are presumed to be distinct and of significance to the segmentation process (see below). An example of these manually defined regions can be seen in Fig. 2(a) and 2(c). A small corridor (20 pixel for the metacarpal bones and 10 pixel for the hearts) is created defining the region around the shape. This area outside the shape contains information about surrounding neighboring structures that is taken into account during classification.

Local image descriptors (e.g. gaussian derivative filters, Gabor filters [16]) are computed for all training images. The region map is warped back to each training shape using Thin Plate Spline Warping (TPS) [17], so that for each region a distribution of the corresponding descriptors/features can be estimated by sampling. The shape model, the region map and the learnt feature descriptors for the regions thus constitute the prior knowledge of Shape Particle Filters.

During search on a test image, a k-NN classifier is used to classify the image's pixels $j \in 1 \dots N_J$ resulting in one region probability map $P(j \mid l)$ per region l. The actual segmentation step uses this probabilities to optimize a fitness function encoding the belief in the segmentation corresponding to a given shape model parameter vector.

This optimization is performed using particle filtering by importance resampling processes [2, 3], estimating the posterior distribution of the shapes given the image by means of the following fitness function (Eq. 7). Initially, a random set of shapes, the particles, represented by shape parameter vectors $\mathbf{c_i}$ are generated according to the distribution of the prior shape model.

The region map is deformed according to the shape parameters and for each region the cumulative probability is computed by summing up the probabilities from the corresponding probability map.

By this, a weight can be applied to each particle considering their likelihood,

$$\pi(\mathbf{c}_i) = \frac{\sum_{l=1}^{L} \sum_{j=1}^{n} P(j \mid l)}{L}, \tag{7}$$

where L is the number of regions, n is the number of pixels in the region map and $P(j \mid l)$ is the probability of pixel j belonging to region l. New particles are generated from the current set of particles by weighting them with their likelihood $\pi(\mathbf{c}_i)$ and randomly sampling in parameter space around these particles with probabilities proportional to the weights. While this importance resampling process is repeated the initial sparse particles evolve into a distribution with high density around the most likely shapes.

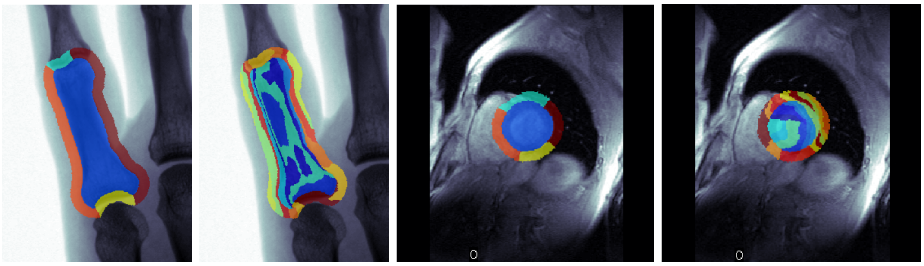

(a) (b) (c) (d)

Fig. 3. Manually predefined and automatically generated region maps for the metacarpal bones (a),(b) and the hearts (c),(d). The automatic results show how the Gabor features are clustered into regions which are considerably different from the ones chosen by humans.

3 Automatic region map generation

The manual definition of the region map represents the introduction of a strong bias, as there is no guarantee that their definition is beneficial or at least suited to the convergence and accuracy of the optimization scheme. In contrast to previous approaches we thus propose a method which derived an optimal region map directly from the training image data. It takes into account the discriminative power of the computed image features and reflects their distribution in the region map.

Similar to the approach in Sec. 2.3 an average feature vector $\mathbf{f}_i$ (Gabor Jets) is computed for each pixel i within the mean shape (as well as within a border around the mean shape) from the corresponding features $\mathbf{f}_i^n$ from each training image $n \in 1 \dots N_S$. The task is now to estimate a sensible partition, i. e. region map, of the inner and outer/border of the mean shape such that the probabilities $P(j \mid l)$ of the image classification using this partition convey information which makes the particle filter converge at a good segmentation. The number of regions within the mean shape is denoted by N_{inner} and the number of regions within the border by N_{border}.

First the feature matrix $\mathbf{F}_n$ for each training image is extracted. Then the mean feature matrix

$$\bar{\mathbf{F}} = \frac{\sum_{n=1}^{N} \mathbf{F}_n}{N_S} \tag{8}$$

is calculated from the individual feature maps after they have been warped onto the mean shape. The area inside the mean shape is clustered into N_{inner} regions and the corridor is clustered into N_{border} regions. The resulting region map with $L = N_{inner} + N_{border}$ regions is for training the classifier and finally for the segmentation step of the Shape Particle Filter.

To obtain the optimal number of regions leave one out cross validation (LOOCV) is used. For each test shape all 100 possible region number combi-

	k-NN	kd-tree + k-NN	linear SVM	speed gain vs. k-NN	speed gain vs. kd-tree + k-NN
Metacarpal bones	641.4	363.8	70.5	9.1x	5.2x
Hearts	239.8	134.8	19.9	12.1x	6.8x

Table 1. Mean classification speed over 10 runs for one test image in seconds for the k-NN, the kd-tree + k-NN and the linear SVM. In the rightmost column the speedup achieved by using SVMs compared to the other classification algorithms is shown (SVM times faster than k-NN and kd-tree + k-NN).

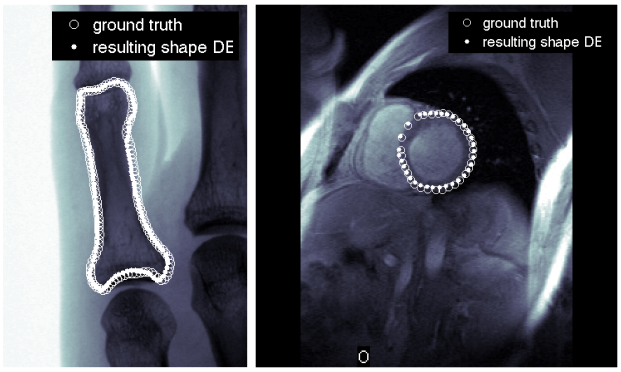

(a) (b)

Fig. 4. Example images of the metacarpal bones (a) and hearts (b) data set with both ground truth and segmentation result. The objects were both automatically localized in the image and delineated.

nations ($N_{inner} \times N_{border}$ where $N_{inner}, N_{border} \in 1, \ldots, 10$) are generated and the segmentation results are computed. By comparing the segmentation results for each region pair and selecting those with the minimal landmark error to ground truth, the optimal number of regions for the region map is determined. Examples of these automatic region maps and manual region maps are shown in Fig. 3.

During the segmentation process the pixels of the target test image are classified using a linear Support Vector Machine (SVM [18, 19, 20, 21]), yielding probabilities for each pixel for belonging to the L regions. By using linear SVMs a major speed up compared to a simple k-Nearest Neighbors (k-NN) approach as well as compared to k-NN in combination with a kd-tree [22] based distance computation could be achieved (see Tab. 1).

4 Experiments

In this section the experimental setup and results, as well as a discussion of the proposed results are presented.

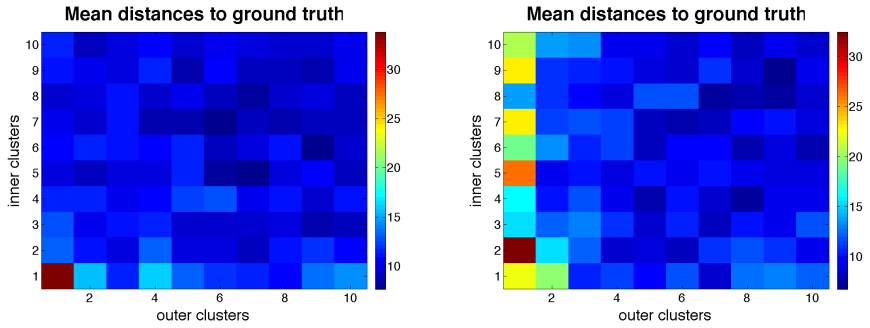

(a) metacarpal bones (b) hearts

Fig. 5. Visualization of the mean landmark error for all evaluated combinations of region numbers over three LOOCV runs for the metacarpal bones (a) and the hearts (b). As can be expected, using a too small number of regions results in poor results as the resulting region probability estimates do not convey enough geometric information for the optimization.

Setup Evaluation was performed on radiographs of metacarpal bones and on MRI slices of the heart. The shapes in the data sets were annotated manually forming the ground truth. For each data set and parameter combination $3N_S$ segmentation runs were performed, i.e. three full leave-one-out cross validations. For the first experiment manually predefined region maps and for the second automatically generated region maps were used as presented in Sec. 3. A SVM with linear kernel was trained for the classification task. The decision for a linear kernel was made to achieve a tradeoff between computational performance and classification result quality. Furthermore the SVM was used to compute probability estimates instead of definite class labels as required for the particle filter segmentation. To eliminate all other factors, the identical optimization scheme using Differential Evolution was used for both experiments, such that the results illustrate the influence of manual vs. automatic region definition only. For each resulting segmentation (see Sec. 2) the mean euclidean distance (mean landmark error) to the ground truth was calculated.

The data sets used for evaluation were **1)** 15 radiographs of human metacarpal bones with the resolution of approximately 500×400 pixels each. **2)** 14 short-axis, end-diastolic cardiac MRI slices of the human heart with the resolution of 256×256 pixels with manually placed landmarks on the epicardial and endocardial contours [23]. Example images for both data sets including ground truth and exemplary segmentation results are shown in Fig. 4.

Results In the comparison of the results that were generated using the manual and automatic region maps the main focus was on the landmark error. As mentioned above the automatic region map leading to the minimal landmark error was obtained using LOOCV over all region combinations. The resulting mean landmark errors for all region pairs of the respective data set are visual-

		median	mean	std
Metacarpal bones	manual	10.12	12.51	9.88
	auto	**4.96**	**7.21**	**6.92**
Hearts	manual	5.80	8.96	11.26
	auto	**4.36**	**5.10**	**3.59**

Table 2. Resulting median, mean and standard deviation of the landmark error in pixel for the metacarpal bones with 12 (5 inner, 7 border) regions and for the hearts with 18 (9 inner, 9 border) regions in the auto region map (our approach) compared to the results obtained using the manually defined region map. Note how the accuracy of the resulting segmentation is considerably increased.

ized in Fig. 5. It can be observed that the results for the automatic regions show that both the number and location of the manual regions are not sufficient to capture the spacial feature distribution in the images. In fact for both data sets good segmentation results were achieved with region combinations from $5 - 9$ inner and border regions.

In Fig. 6 boxplots of the resulting landmark errors for all four distinctive runs (manual vs. automatic region map each for the metacarpal bones and the hearts) are shown. For the metacarpal bones a auto region map with 5 inner and 7 border regions and for the hearts a region map with 9 inner and 9 border regions led to the best segmentation results and therefore to the minimal landmark error. Therefore the following key values in pixel for the different data sets could be achieved: The median of the landmark error for the metacarpal bones could be reduced from 10.12 to 4.96 and for the hearts from 5.8 to 4.36. The mean landmark error did also decrease for the metacarpal bones from 12.51 to 7.21 and for the hearts from 8.96 to 5.10. The standard deviation of the landmark error for the metacarpal bones was reduced from 9.88 to 6.92 and for the hearts from 11.26 to 3.59. A summary of these values is shown in Table 2.

Discussion The quality of the generated results depends on four major factors besides the used region map. These are the image quality of the used input data (that in turn influences the extracted image features), overlaps of or no space between nearby similar structures, the accuracy of the manually annotated ground truth as well as the accuracy of the used image classification scheme. Input image quality is used as a collective term for the amount of noise, shadows of overlapping anatomical structures or other distortions due to the image creation process.

The approach using automatically generated region maps outperformed the manually defined version especially on images with low input image quality. Due to the better incorporation of the feature information of the structure and its surroundings, the auto region maps lead to more precise classifications and therefore to more exact segmentation results. Furthermore the manual region maps could not provide the necessary level of detail to cope with nearby or overlapping similar structures because of the lack of distinctive regions in crucial image areas. In particular this was observed on the metacarpal bones data set, where

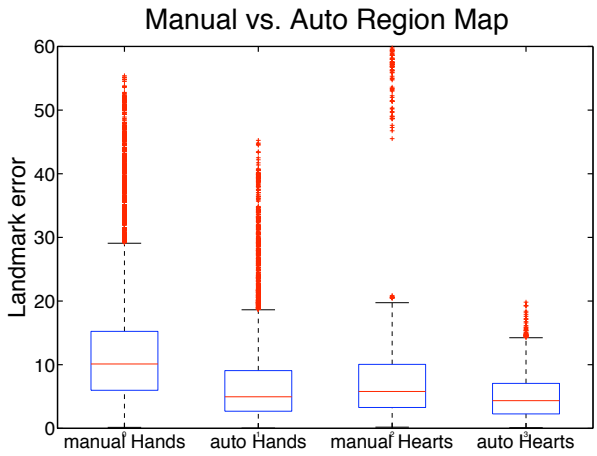

Fig. 6. Boxplots of the results for the image segmentation using manually and automatically generated region maps for the metacarpal bones and the hearts data sets. Using the automatic region estimation results in fewer outliers and higher accuracy, displaying the effectiveness of the proposed approach.

the main problem arose at the distal bone region i.e. the joint area where extreme narrow inter-bone spaces appeared. A selection of different image features incorporating local structures or even automatically learned features for these areas could lead to a better segmentation accuracy.

5 Conclusion

In this work we have shown that using manually defined region maps for shape particle filtering introduces a bias which reduces segmentation accuracy considerably. By using region maps which are automatically derived through clustering in the feature space the optimal number and distribution of inner and outer regions is found, leading to substantially increased accuracy, as shown on the two medical data sets. Furthermore, the laborious estimation of a suitable manual region map trough trial and error is eliminated, paving the way to rapid application of Shape Particle Filters in clinical scenarios. Future work will focus on the investigation of the optimal selection of feature types for specific target objects. The method's extension to 3D will allow to use its capability to localize and segment anatomical structures to further modalities.

References

[1] Seise, M., Mckenna, S.J., Ricketts, I.W., Wigderowitz, C.A.: Parts-based segmentation with overlapping part models using markov chain monte carlo. Image and Vision Computing **27**(5) (Feb 2009) 504–513

[2] de Bruijne, M., Nielsen, M.: Shape particle filtering for image segmentation. Proc. MICCAI 2004 **3216** (Jan 2004) 168–175
[3] de Bruijne, M., Nielsen, M.: Image segmentation by shape particle filtering. Proc. ICPR **3** (2004) 722–725
[4] Bruijne, M.D., Nielsen, M.: Multi-object segmentation using shape particles. Lecture Notes in Computer Science: Information Processing in Medical Imaging **3565** (Jan 2005) 762–773
[5] de Bruijne, M.: Shape particle guided tissue classification. Mathematical Methods in Biomedical Image Analysis (MMBIA) (Apr 2006) 8
[6] Doucet, A., Freitas, N.D., Gordon, N.: Sequential monte carlo methods in practice. Springer (Jan 2001) 581
[7] Liebelt, J., Schertler, K., Germany, E.: Precise registration of 3d models to images by swarming particles. CVPR (2007)
[8] Sørensen, L., Østergaard, J., Johansen, P., Bruijne, M.D.: Multi-object tracking of human spermatozoa. Proceedings of SPIE (Jan 2008)
[9] Gordon, N., Salmond, D., Smith, A.: Novel approach to nonlinear/non-gaussian bayesian state estimation. IEEE Proceedings for Radar and Signal Processing **140**(2) (Jan 1993) 107–113
[10] Fearnhead, P.: Sequential monte carlo methods in filter theory. (Jun 2008)
[11] Cootes, T., Taylor, C., Cooper, D., Graham, J.: Training models of shape from sets of examples. In Proc. British Machine Vision Conference (Jan 1992) 9–18
[12] Thodberg, H.H.: Minimum description length shape and appearance models. Proceedings of Information Processing and Medical Imaging (2003)
[13] Cootes, T., Taylor, C.: Statistical models of appearance for computer vision. World Wide Web Publication (Jan 2001)
[14] Braak, C.: A markov chain monte carlo version of the genetic algorithm differential evolution: easy bayesian computing for real parameter spaces. Stat Comput **16**(3) (Jan 2006) 239–249
[15] Storn, R., Price, K.: Differential evolution – a simple and efficient heuristic for global optimization over continuous spaces. Journal of Global Optimization **11**(4) (Jan 1997)
[16] Yoshimura, H., Etoh, M., Kondo, K., Yokoya, N.: Gray-scale character recognition by gabor jets projection. Proc. ICPR **2** (Jan 2000) 335–338
[17] Bookstein, F.: Principal warps: thin-plate splines and the decomposition of deformations. Pattern Analysis and Machine Intelligence, IEEE Transactions on Pattern Analysis and Machine Intelligence **11**(6) (Jun 1989) 567 – 585
[18] Vapnik, V.N.: The nature of statistical learning theory. Springer (2000)
[19] Burges, C.: A tutorial on support vector machines for pattern recognition. Data mining and knowledge discovery (Jan 1998)
[20] Scholkopf, B., Smola, A., Williamson, R., Bartlett, P.: New support vector algorithms. Neural Computation (Jan 2000)
[21] Bishop, C.M.: Pattern recognition and machine learning. Springer (Jan 2006)
[22] Bentley, J.: Multidimensional binary search trees used for associative searching. Communications of the ACM **18**(9) (Jan 1975) 509 – 517
[23] Stegmann, M., Fisker, R., Ersboll, B.: Extending and applying active appearance models for automated, high precision segmentation in different image modalities. Proceedings of the Scandinavian Converence on Image Analysis (Jan 2001)